Experimental study of the β-delayed neutron decay of ^{21}N

Z. H. Li, J. L. Lou, Y. L. Ye,* H. Hua, D. X. Jiang, X. Q. Li, S. Q. Zhang, T. Zheng, Y. C. Ge, Z. Kong, L. H. Lv, C. Li, F. Lu, F. Y. Fan, Z. Y. Li, Z. X. Cao, L. Y. Ma, and Q. Faisal

School of Physics and State Key Laboratory of Nuclear Physics and Technology, Peking University, Beijing 100871, People's Republic of China

H. S. Xu, Z. G. Hu, M. Wang, X. G. Lei, L. M. Duan, Z. G. Xiao, W. L. Zhan, G. Q. Xiao, T. H. Huang, F. Fu, X. H. Zhang, C. Zheng, Y. H. Yu, X. L. Tu, Y. P. Zhang, Y. Y. Yang, H. B. Zhang, B. Thang, Y. L. Tian, Z. Ouang, M. R. Huang, Z. G. Xu, K. Yue, and Q. Gao

Institute of Modern Physics, Chinese Academy of Sciences, Lanzhou 730000, People's Republic of China

(Received 22 December 2008; revised manuscript received 16 August 2009; published 24 November 2009)

The first spectroscopic study for the β decay of ^{21}N is carried out based on β-n, β-γ, and β-n-γ coincidence measurements. The neutron-rich ^{21}N nuclei are produced by the fragmentation of the $E/A = 68.8$ MeV ^{26}Mg primary beam on a thick ^{9}Be target and are implanted into a thin plastic scintillator that also plays the role of β detector. The time of flight of the emitted neutrons following the β decay are measured by the surrounding neutron sphere and neutron wall arrays. In addition, four clover germanium detectors are used to detect the β-delayed γ rays. Thirteen new β-delayed neutron groups are observed with a total branching ratio of $90.5 \pm 4.2\%$. The half-life for the β decay of ^{21}N is determined to be 82.9 ± 7.5 ms. The level scheme of ^{21}O is deduced up to about 9 MeV excitation energy. The experimental results for the β decay of ^{21}N are compared to the shell-model calculations.

DOI: 10.1103/PhysRevC.80.054315 PACS number(s): 23.40.−s, 23.20.Lv, 27.30.+t

I. INTRODUCTION

Studies of β decay of nuclide provide rich information on the nuclear structure of the mother and daughter nuclei. Especially for nuclei close to the drip line, β decay may release a large amount of energy and can populate the highly exited states of the daughter nuclide with relatively high probability. The spectroscopic information obtained with this method is important since the effective interaction between nucleons changes when the neutron or proton number increases along the isotopic chain toward the drip line. Also β decay of nuclei far from the stability line plays an important role in processes such as stellar evolution.

β decay of neutron-rich unstable nuclide often results in delayed neutron and γ emissions from the excited daughter and granddaughter nuclei. Therefore, the coincident measurement of β-n-γ particles is generally required to unambiguously assign the quantum-state properties of the related nuclei.

Recently, oxygen isotopes attracted particular interest in terms of nuclear structure because of the change of the subshell closures at neutron numbers $N = 14$ and $N = 16$ [1]. The experimental studies of oxygen isotopes were carried out using the β-delayed neutron spectroscopy method for ^{18,19,20}O at the National Superconducting Cyclotron Laboratory (NSCL) [2,3] and for ^{18}O at Peking University [4,5]. Extending the studies to heavier oxygen isotopes closer to the neutron drip line is important to understanding the systematic structure evolution of the unstable nuclei. For the neutron-rich nucleus ^{21}N, the β decay energy is as high as 17.19 MeV, which lies well above the single-neutron separation energy ($S_n = 3.81$ MeV) and two-neutron separation energy ($S_{2n} = 11.41$ MeV) of the daughter nucleus ^{21}O. Thus, the delayed emission of single or double neutrons may occur. In 1990, Mueller *et al.* [6] reported the half-life and β-delayed neutron emission branching ratio of ^{21}N to be 95^{+11}_{-15} ms and $84 \pm 9\%$, respectively. In 1995, based on a new measurement, Reeder *et al.* [7] gave these values as 83.6 ± 6.7 ms and $78 \pm 7\%$, respectively. An early study by Catford *et al.* [8] used the ^{18}O (^{18}O,^{15}O) ^{21}O transfer reaction to identify four excited states in ^{21}O. Recently, the level scheme below 4.92 MeV excitation energy in ^{21}O was established [9] using fragmentation reactions. So far, the observed highest energy state is only about 1 MeV above the neutron separation energy. Stanoiu *et al.* [9] assigned the spin and parity of these observed excited states based on a shell-model calculation.

For the first time we present here the spectroscopic information of β decay of the neutron-rich nucleus ^{21}N based on β-n, β-γ, and β-n-γ coincidence measurements and we try to establish the level scheme of ^{21}O up to about 9 MeV excitation energy.

II. EXPERIMENTAL SETUP

The primary beam of ^{26}Mg at 68.8 MeV/nucleon was provided by the Heavy Ion Research Facility in Lanzhou (HIRFL) and impinged on a ^{9}Be primary target with a thickness of 303 mg/cm^2. The secondary beam of ^{21}N was separated, purified, and collected by the Radioactive Ion Beam Line in Lanzhou (RIBLL) [10]. In the upper part of Fig. 1 an overall view of the whole detection system is shown, with its inner details presented in the lower part. The secondary beam of ^{21}N passes through a thin Kapton window, which separates the beam line vacuum from the air. A 325-μm-thick

*yeyl@pku.edu.cn

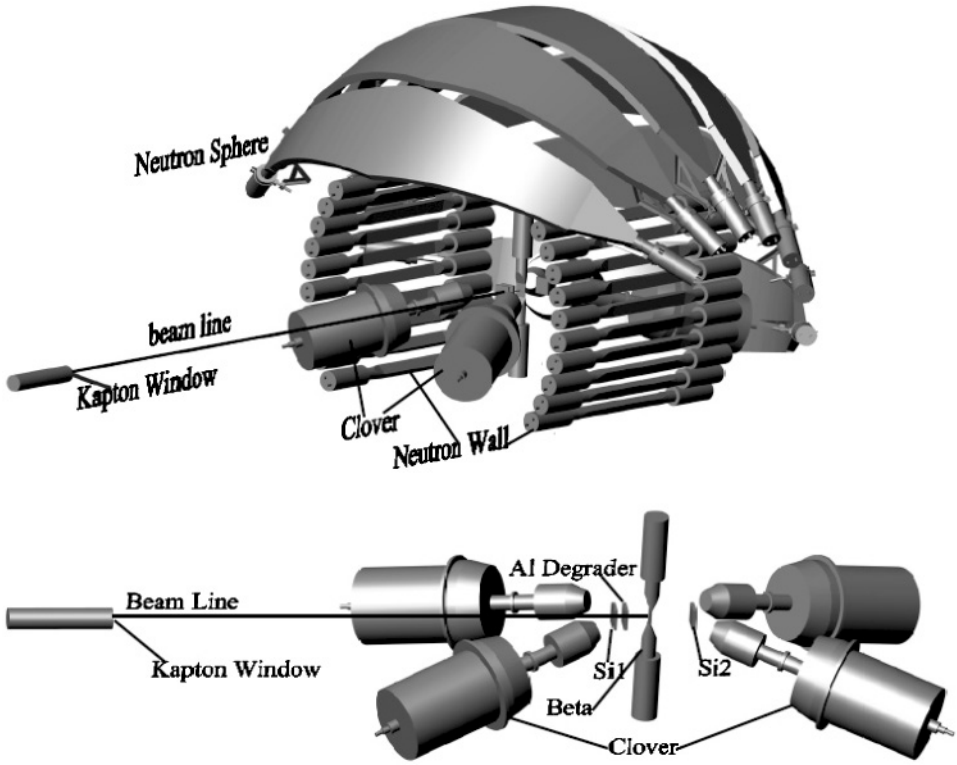

FIG. 1. The experimental set-up for measuring the β-delayed neutron and γ decay of ^{21}N, with the upper part an overall view of the whole system and the lower part its inner details.

silicon ΔE detector (Si1) is located about 1 m downstream of the Kapton window. The beam energy is reduced by an aluminum energy degrader before being fully absorbed by an implantation detector made of an NE102 plastic scintillator with an area of 4.0 $\times$ 5.0 cm^2 and a thickness of 3 mm. The implantation detector, located at the center of the detection system, also played the role of β detector. The mean time of two timing signals taken from both ends of the implantation detector is used as the starting time for the time-of-flight (TOF) measurement of the emitted neutrons. Another silicon detector (Si2), with a thickness of 325 μm, is placed downstream of the implantation detector to veto the ions that escape from the implantation detector.

The energy loss in ΔE detectors (Si1 and Si2) combined with the TOF in RIBLL provides the online particle identification of the incoming particles, as shown in Fig. 2. It is found that the nuclei with mass numbers $A < 15$, which contribute 45.6% of the secondary beam, pass through the implantation detector and can be eliminated by the veto detector Si2. The secondary beam stopped in the implantation detector has an intensity of about 0.5 particle per second (pps) with an isotopic purity of 74.5% for ^{21}N and some small percentages for other contaminant impurities, as presented in the upper part of Fig. 2(a). During the experiment, ^{16}C and ^{17}N beams are also periodically selected by RIBLL to calibrate detection efficiency for the neutron detection arrays and the γ detectors, as described in the following.

The β-delayed neutrons from the β decay of ^{21}N are detected in coincidence with β rays by using two types of neutron detector arrays, namely a neutron sphere and a neutron wall, which provide the stopping time for neutron TOF measurements.

The neutron sphere is designed for the detection of neutrons with relatively high energies ($\gtrsim$1 MeV). It is composed of eight identical plastic scintillation bars (BC408) [11]. Each counter has a length of 157 cm and is curved to a radius of 100 cm to have the same flight path length for neutrons emitted from the implantation detector. The thickness of each scintillator is 2.5 cm and the width is 40 cm at the middle of the bar and 20 cm at both ends. Each end is coupled to an EMI-9214B photomultiplier tube (PMT) via a light guide. The total solid angle of this detector array is approximately 30% of 4π sr. The neutron wall is designed mainly for the detection of low-energy neutrons, which consist of 20 short plastic scintillation bars (40.0 cm in length, 4.5 cm in width, and 2.5 cm in thickness). Each end of the bar is coupled to a XP2020 PMT via a light guide. As shown in Fig. 1, the neutron wall is installed inside the neutron sphere, located about 62 cm away from the implantation detector, and covered 8% of 4π sr.

The flight path length, response function, and detection efficiencies for these two neutron-detector arrays are calibrated by using the observed neutron peaks corresponding to the well-known β-delayed neutron decay of ^{17}N with neutron energies at 383, 1170, and 1700 keV and of ^{16}C with neutron energies at 808, 1715, and 3290 keV. For a detailed analysis of the calibration, including the detection and description of the neutron spectra as a function of neutron energy, see the recently published article by Lou *et al.* [12]. We show here only the detection efficiencies for the neutron sphere and the neutron wall (Fig. 3). In addition to the experimental results, three Monte Carlo simulation points at 1.7, 2.5, and 4.5 MeV, calculated with the code KSUEFF [13], are also plotted in the figure. The data points are fitted by an efficiency curve. For the neutron sphere, the uncertainties of the efficiencies for

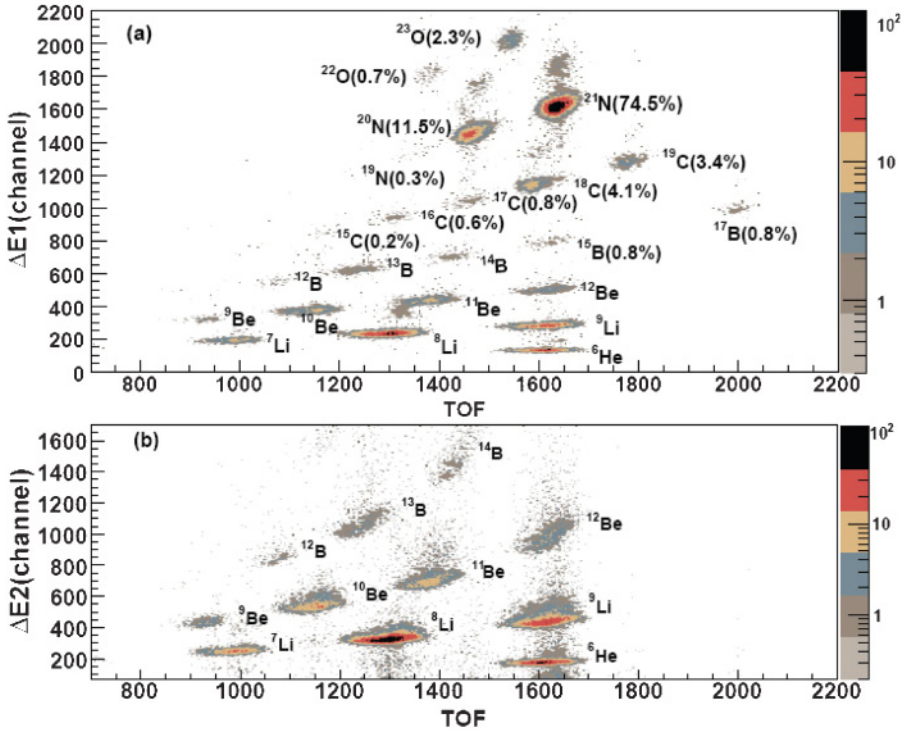

FIG. 2. (Color online) Particle identification plot for incoming particles. (a) Energy loss in the Si1 detector versus TOF in RIBLL; (b) the same as (a) but with the Si2 detector.

the energies above and below 0.8 MeV are expected to be about 10% and 20%, respectively. For the neutron wall, the uncertainties for the energies above and below 0.3 MeV are about 10% and 20%, respectively.

The β-delayed γ rays were detected by four clover germanium detectors placed 12 cm away from the implantation detector. The detection efficiencies are determined using radioactive sources such as ^{60}Co, ^{207}Bi, and ^{152}Eu. The known β-delayed γ rays of ^{17}N and ^{19}O (the impurity for the ^{16}C beam) are also used for efficiency calibration. The detection efficiency curve for one clover detector is shown in Fig. 4.

Since the beam intensity is very low (about 0.5 pps for ^{21}N), the experimental data are taken in a new random beam-on/beam-off cyclical mode, in contrast to the previously used periodical mode [4]. When an incoming particle was detected by the ΔE detector during the beam-on period, the data acquisition system was triggered. To reduce the background counting rate caused by impurity beams, a ΔE-TOF window was applied by the electronics circuit to basically select the ^{21}N ions. Once such an event was triggered, the primary beam was turned off by a beam chopper [14] for a period of 300 ms. The length of the beam-off period was set to approximately

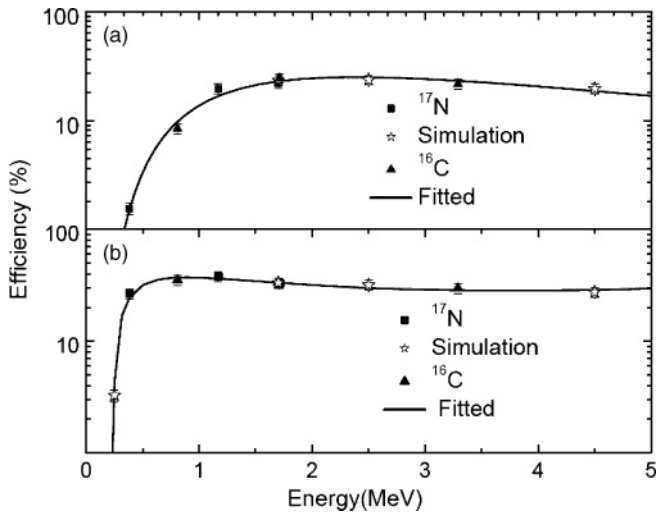

FIG. 3. Neutron detection efficiencies as a function of neutron energy for the neutron sphere (a) and the neutron wall (b). The solid curve is a fit to the experimental and simulation data points.

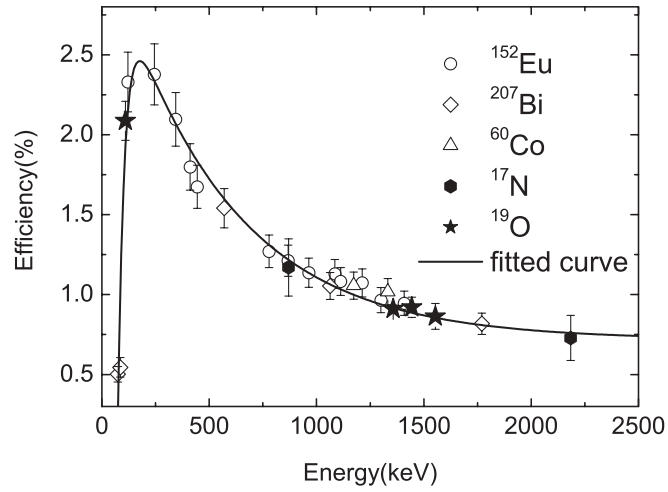

FIG. 4. γ detection efficiency as a function of γ energy for one clover detector. The empty dots and solid dots are experimental results obtained by using a radioactive source and an implanted beam, respectively. The solid curve is a fit to the experimental data.

three times the half-life of ^{21}N [7]. During the beam-off period the signals from the β detector, neutron detector arrays, and γ detectors were recorded.

III. ANALYSIS AND DISCUSSION

A. The half-life of ^{21}N

The inclusive β-decay curve of ^{21}N, obtained from the time difference between the implantation timing signal and the β-particle signal during the beam-off period, is used to determine the half-life of ^{21}N. Nearly all the implanted nuclide and their daughters and granddaughters are included in the growth and decay calculations of these nuclei. In the calculations, the half-lives of ^{15}B, ^{17}B, ^{18}C, ^{19}C, ^{20}N, and ^{23}O are fixed at known values of 9.93, 5.08, 66, 45.5, 130, and 82 ms, respectively, as obtained from Ref. [15]. The contributions from various daughters and granddaughters, generally having longer lifetimes, are calculated by using their half-lives and β-delayed neutron emission branching ratios obtained from Ref. [15]. The radioactive nuclei that do not decay within the actual cycle are added to the next cycle. For nuclei with much longer half-lives, such as ^{22}O and so on, the activities approach saturation just a few minutes after the start of the experiment run. This kind of contribution may generally be considered as a constant background [3]. At the end, only four parameters are left as variables to be determined: the half-life, the initial activity, the neutron emission probability P_n of ^{21}N, and a constant background. The fitting is obtained with a reduced χ^2 value of 0.987, as shown in Fig. 5. The half-life value of 82.9 $\pm$ 7.5 ms and the total number of decay events of 1.49 $\times$ 10^5 are obtained from the fitting.

B. Analysis of neutron spectra

The TOF spectra for β-delayed neutrons recorded by the neutron sphere and neutron wall are shown in Figs. 6(a) and 6(b), respectively. To illustrate the results in a comparable

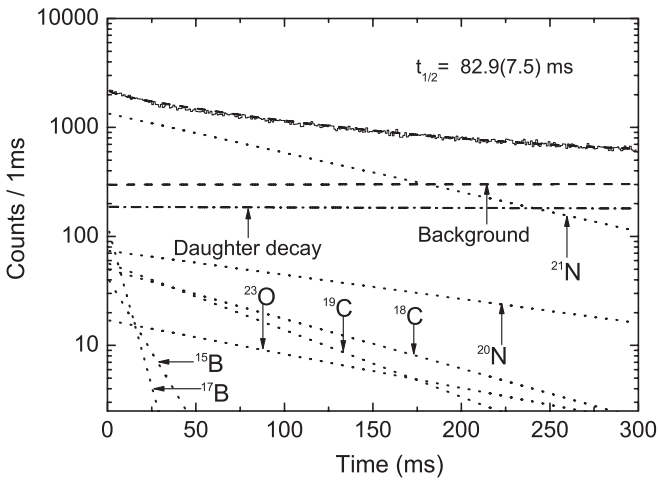

FIG. 5. The inclusive β-decay curve for ^{21}N. The total decay curve (solid line), various decay components of the implanted impurity nuclei (dotted line), decay contribution from all daughter nuclei (dot-dashed line), and a constant background (dashed line) are included in the analysis.

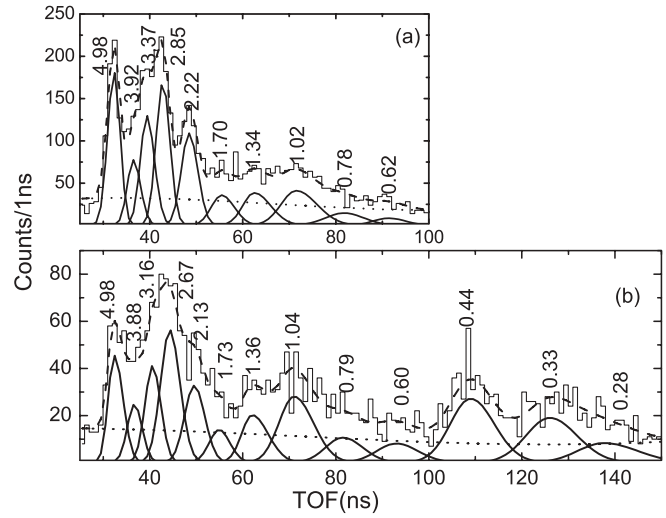

FIG. 6. The TOF spectra measured by the neutron sphere (a) and the neutron wall (b). The data are fitted with asymmetric Gaussian function plus a cubic background. The neutron energies are given in MeV.

scale, the flight paths of all neutron detectors are normalized to 1 m. Time zero is deduced from the position of a sharp peak generated by relativistic electrons, which is not shown in the spectra. Compared to the neutron wall, the neutron sphere with a longer flight path and larger solid angle coverage has better time resolution and higher statistics for neutron groups at relatively high energies; however, the detection efficiency for neutron groups below 600 keV decreases rapidly, as shown in Fig. 3. Fortunately, the low-energy part can be recovered by the neutron wall, as shown in Fig. 6(b), due to its advantage of having a much lower detection threshold. The spectra are then fitted by asymmetric Gaussian peak functions plus a cubic background, using the program PEAKFIT. The peak width and asymmetric shape factor for each peak are determined from the calibration data with ^{16}C and ^{17}N beams. The detailed description of the calibration can be found in Ref. [12]. At the starting point, five relatively high energy peaks between 5.0 and 2.2 MeV are identified in the spectrum for the neutron sphere, whereas four peaks at about 1.36, 1.04, 0.44, and 0.33 MeV are set in the spectrum for the neutron wall (Fig. 6). Then, to consistently describe both spectra for the neutron sphere and the neutron wall and to obtain a good χ^2 value in the fit, it is necessary to add peaks at about 1.70, 0.79, 0.60, and 0.28 MeV, constrained by the pulse shape determined by the calibration. The peak positions, as well as the peak width and asymmetry factors [12], are then varied to fit the neutron TOF spectra. Finally, 13 neutron groups are obtained with the minimum reduced χ^2 value of 0.97 for the neutron sphere and 0.88 for the neutron wall.

Figure 7 shows the typical β-decay curves gated by the major neutron peaks with sufficient statistics. These spectra are fitted with a single exponential function and a constant background. The extracted half-lives displayed in Fig. 7 are in agreement with each other and with those obtained from the inclusive data within the error bar. This provides complementary evidence for the origin of these neutrons.

TABLE I. Summary of the experimental results for the β-delayed neutron and γ decay of ^{21}N.

Peak energy (MeV)	E_x (^{21}O) (MeV)	BR (%)	Log (ft)	B (GT) $\times$ 1000	J^π
1.222 ± 0.003[a]	1.222±0.003	3.5 ± 0.4	6.45 ± 0.06	2.2 ± 0.3	$1/2^+, 3/2^+, 5/2^+$
4.98 ± 0.22[b]	9.04 ± 0.22	9.9 ± 1.1	4.62 ± 0.06	146.2 ± 20.6	$1/2^-, 3/2^-$
3.92 ± 0.15[b]	–	4.1 ± 0.5	–	–	–
3.37 ± 0.12[b]	9.02 ± 0.12	6.9 ± 0.8	4.78 ± 0.06	101.5 ± 14.5	$1/2^-, 3/2^-$
2.85 ± 0.10[b]	6.80 ± 0.10	8.4 ± 0.9	5.19 ± 0.06	39.9 ± 5.6	$1/2^-, 3/2^-$
2.22 ± 0.08[b]	6.14 ± 0.08	6.3 ± 0.7	5.44 ± 0.06	22.4 ± 3.2	$1/2^-, 3/2^-$
1.73 ± 0.07[c]	–	2.7 ± 0.4	–	–	–
1.36 ± 0.07[c]	6.91 ± 0.07	4.5 ± 0.6	5.44 ± 0.07	22.4 ± 3.5	$1/2^-, 3/2^-$
1.04 ± 0.06[c]	–	7.8 ± 0.9	–	–	–
0.79 ± 0.04[c]	–	3.4 ± 0.5	–	–	–
0.60 ± 0.03[c]	–	3.1 ± 0.5	–	–	–
0.44 ± 0.02[c]	–	12.9 ± 1.5	–	–	–
0.33 ± 0.01[c]	–	13.0 ± 2.7	–	–	–
0.28 ± 0.01[c]	–	7.7 ± 1.7	–	–	–

[a] β-delayed γ emission.
[b] β-delayed neutron emission measured by the neutron sphere.
[c] β-delayed neutron emission measured by the neutron wall.

The branching ratio (BR), together with the error, for each neutron group is then obtained by using the net neutron peak counting, the corresponding neutron detection efficiency, and the total number of observed decay events. Both neutron peak energies and branching ratios measured by the neutron sphere are consistent with those measured by the neutron wall within the error bars. The results are summarized in Table I. The obtained total neutron emission branching ratio P_n is $90.5 \pm 4.2\%$, which is in agreement with previously reported values of $84 \pm 9\%$ [6], within the error bar.

C. Analysis of γ spectra

In Fig. 8 the γ spectrum measured in coincidence with the β decay of ^{21}N during the beam-off period by all four Ge clover detectors is shown. The identified peaks are labeled with energies in keV and its parent nucleus. The assignments are made based on the experimentally known γ transitions and intensities of possible daughters or granddaughters and the γ-gated β-decay half-lives.

The γ-ray transition at an energy of 1222 keV was reported in Ref. [9] and identified as the transition from the first excited state to the ground state of ^{21}O. Other γ-ray peaks for ^{21}O reported in Ref. [9] are not observed in the present experiment. The γ rays at energies of 1674, 2397, 2780, and 3175 keV are related to the excited state of ^{20}O [3,9], which is the granddaughter nucleus following β and neutron decay of ^{21}N. The γ ray at an energy of 2780 keV was not seen in Ref. [9], possibly due to its weak population in fragmentation reactions. The β-decay curves gated by γ rays are displayed in Fig. 9. Again, the half-lives are determined from a fit using a single exponential function and a constant background. The resulting half-lives labeled in Fig. 9 are again consistent with each other and with those obtained from the inclusive spectrum, providing evidence for the origins of these γ rays.

The γ emission probabilities are calculated using the peak counting and the detection efficiencies and normalized to the total number of ^{21}N decay events. The total branching ratio of the β-delayed γ emission of ^{21}N, P_γ, measured in the present work is $3.5 \pm 0.4\%$. The decay chain assignment and emission probability for each β-delayed γ ray are summarized in Table II.

D. Two-neutron emission and triple coincidence

Two-neutron emission is energetically allowed in the β decay of ^{21}N, but it has not been observed so far. If this process exists, the populated ^{19}O grand state will decay to an excited state of ^{19}F, which will emit a 1356 keV γ ray with 50.4% probability [16]. Therefore, the two-neutron emission probability can be estimated from the number of 1356 keV photons. As shown by the inset in Fig. 8(b), a small γ peak at 1356 keV is observed in the present experiment. But this γ ray might also be attributed to the β-delayed neutron decay of the impurity nucleus ^{20}N. It is found that the observed number of 1356 keV γ rays can fully be explained by the β-delayed neutron decay of ^{20}N during the beam-off period. Therefore, we conclude that the β-delayed two-neutron emission is not observed in the present experiment.

To determine the cascade relationship in the decay scheme, we try to perform β-n-γ triple coincidence analysis. Because of the low statistics, the neutron wall data are not used in

TABLE II. The decay chain assignments and the emission probabilities of β-delayed γ rays of ^{21}N.

Energy (keV)	Nuclide	Decay chain assignment	Emission probability (%)
1222 ± 3	^{21}O	^{21}N(β)	3.5 ± 0.4
1674 ± 3	^{20}O	^{21}N(βn)	35.6 ± 5.1
2397 ± 4	^{20}O	^{21}N(βn)	4.5 ± 0.7
2780 ± 4	^{20}O	^{21}N(βn)	2.6 ± 0.6
3175 ± 5	^{20}O	^{21}N(βn)	2.0 ± 0.5

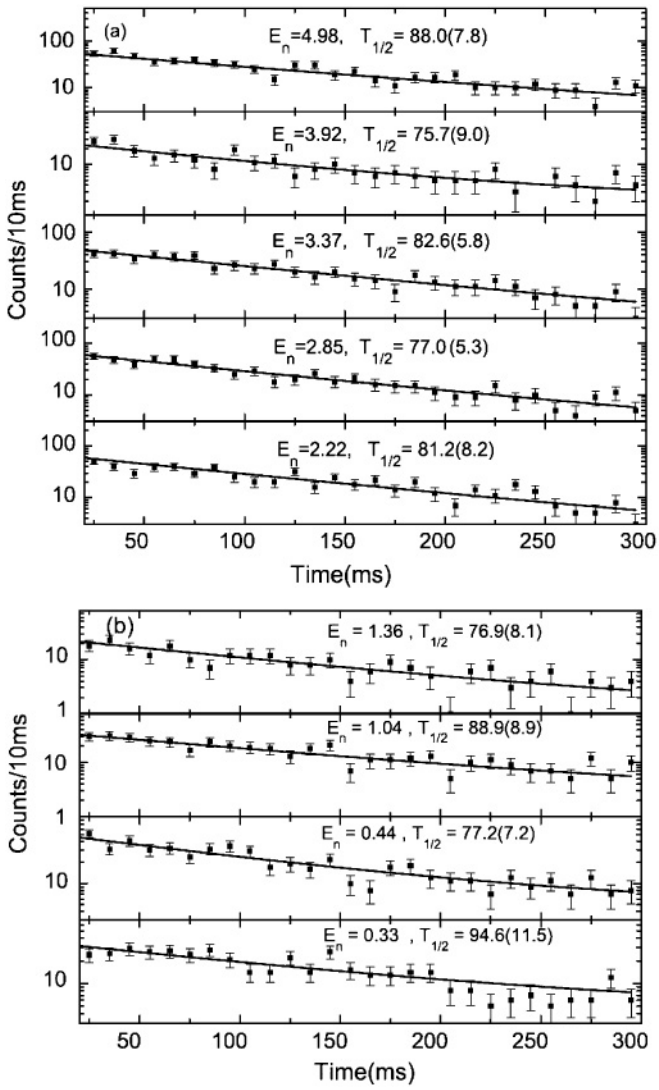

FIG. 7. Typical β-decay curves gated by neutron peaks observed by the neutron sphere (a) and the neutron wall (b). The corresponding neutron peak energies are given in MeV and half-lives in milliseconds.

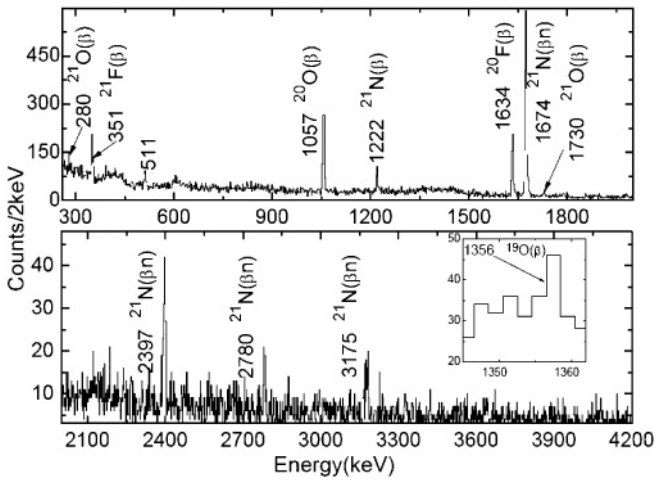

FIG. 8. The γ spectrum measured by all four Ge clover detectors. The energies are given in keV for each peak.

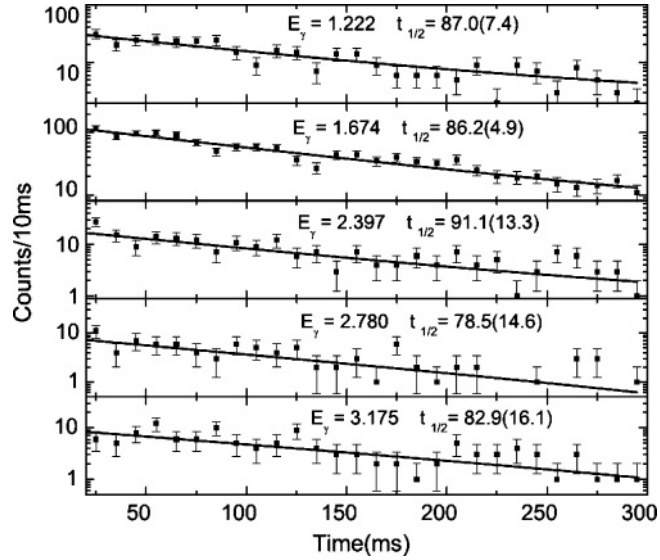

FIG. 9. β-decay curves gated by γ peaks emitted from the β decay of ^{21}N. The corresponding γ energies are given in MeV and half-lives in milliseconds.

this analysis. Figure 10 shows the ungated neutron spectrum following the β decay of ^{21}N, taken by the neutron sphere, in comparison to that gated by the 1674 keV γ rays, which are emitted from the first excited state of ^{20}O. It can be seen that two neutron peaks at 3.37 and 1.34 MeV are in good coincidence with the 1674 keV γ peak. If we take an average background counting as one count per channel, as seen in the gated spectrum, the confidence level for the existence of the coincident peak is 99% at 3.37 MeV and 94% at 1.34 MeV, respectively. From the transition probability point of view, the 2397 keV γ ray might also be related to the 1.34 MeV neutron. The difference of γ detection efficiency between 1674 and 2397 keV is only about 10%. However, no statistically significant peak around 1.34 MeV is observed in the neutron TOF spectrum gated by 2397 keV γ rays, in contrast to that gated by 1674 keV γ rays, as described

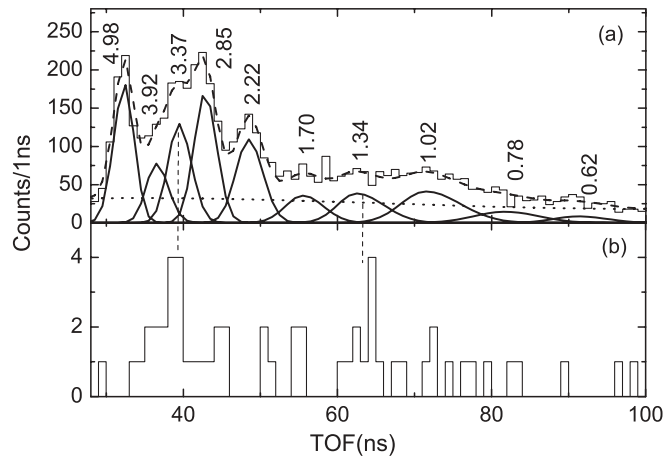

FIG. 10. β-n-γ coincidence analysis. (a) Neutron TOF spectrum following the β decay of ^{21}N, taken by the neutron sphere; (b) the same as (a) but gated with the 1674 keV γ rays.

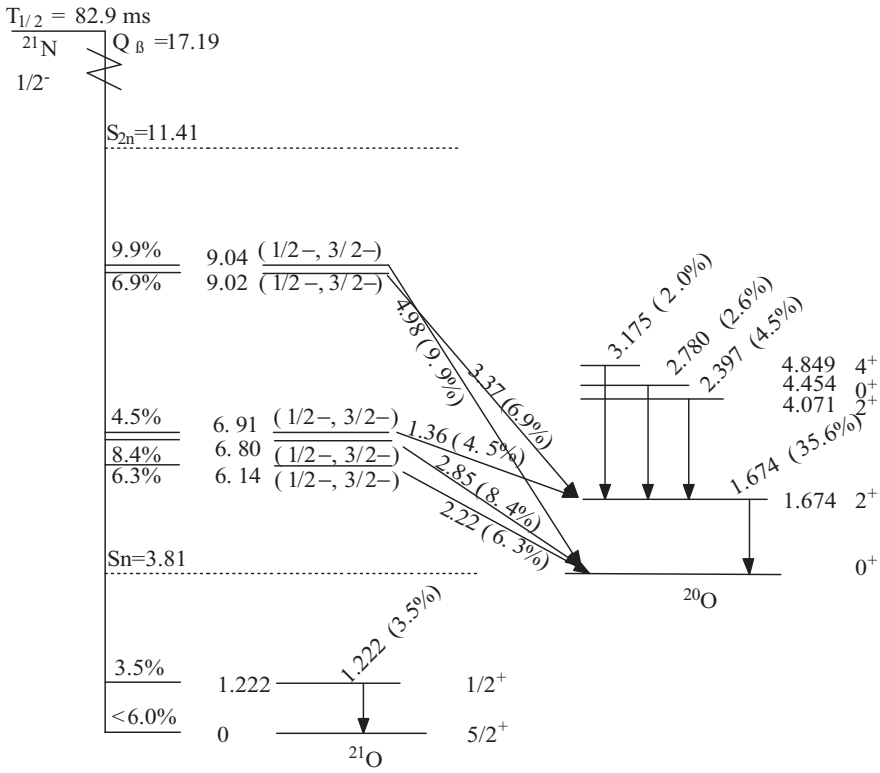

FIG. 11. The decay scheme of ^{21}N. All energies are given in MeV.

previously. Furthermore, the strong neutron peaks at 4.98, 2.85, and 2.22 MeV observed in the ungated spectrum do not have statistical significance in the gated spectrum. In addition, these three neutron peaks cannot fulfill the intensity requirements of any higher exited states of ^{20}O. Therefore, it is suggested that the neutron peaks at 1.34 MeV (1.36 MeV determined by the neutron wall) and 3.37 MeV are related to the first excited state of ^{20}O whereas the neutron peaks at 4.98, 2.85, and 2.22 MeV are related to the ground state of ^{20}O. Because of the very low statistics it is difficult to draw the same kind of assignment for other γ peaks.

E. Overall analysis and results

The established decay scheme of ^{21}N determined from the present work is given in Fig. 11. The excitation energies of ^{21}O are calculated by taking into account the recoil energy of the daughter nucleus.

The upper limit of the β-decay branching ratio feeding to the ground state of ^{21}O is estimated to be $6.0 \pm 4.3\%$ from $1 - P_n - P_\gamma$, where P_n and P_γ represent the branching ratio feeding the neutron unbound and bound excited states of ^{21}O, respectively, as listed in Table. I. Since the neutron detection has a threshold at about 200 keV, this estimation may suffer from the loss of some P_n value for low-energy neutron groups. As an independent verification, we can also deduce the branching ratio feeding the ground state of ^{21}O from the observed 280 keV γ ray. This γ ray results from the β decay of ^{21}O to the first excited state of ^{21}F with a known probability of 14.8% [15]. By using the number of 280 keV γ rays, the detection efficiency and the branching ratio, and by taking into account the growth and decay of ^{21}O during successive beam-off periods, we are able to extract the branching ratio of ^{21}O β decay to be $11.6 \pm 2.2\%$, which is equal to the sum of the branching ratio feeding the bounded excited state and ground state of ^{21}O. By subtracting the γ decay probability of $3.5 \pm 0.4\%$, the β decay branching ratio to the ground state of ^{21}O is estimated to be $8.1 \pm 2.3\%$, which is consistent with the preceding value of $6.0 \pm 4.3\%$ within the error bar. This cross-check also eliminates any significant neutron groups at energies lower than 200 keV.

The log(ft) values and B(GT) values listed in Table I are calculated from the half-life of ^{21}N and branching ratios for the observed states of ^{21}O. The spin and parity of the state at 1222 keV were assigned as $1/2^+$ in Ref. [9]. The presently observed log(ft) value of 6.45 for the β decay to this state indicates that this transition is of a type first forbidden, which limits the spin and parity of this state to $1/2^+$, $3/2^+$, and $5/2^+$, in agreement with the previous assignment. Based on the observed log(ft) values which are in the range between 4.62 to 5.44, the β-decay feeding to all observed neutron unbound states are assigned as allowed β decay with the spin-parity of the final state in ^{21}O to be $1/2^-$ or $3/2^-$.

A preliminary shell-model calculation for allowed β decay of ^{21}N is performed in a "psd" (1p1/2,1p3/2,1d3/2, 1d5/2,2s1/2) model space using WBT interaction (the spsdpf interaction based on the 45-parameter MI-LC psd fit) with the computer code OXBASH [17]. The calculation predicted a half-life of $T_{1/2} = 70$ ms for the β decay of ^{21}N, which is smaller than the experimental value of 82.9 ± 7.5 ms obtained from the present work. The calculation predicts a total neutron emission branching ratio of 90.0% for the ^{21}N β decay to ^{21}O unbound states up to two-neutron separation energy S_{2n}, and the number of the unbound states with a branching ratio larger than 1.0% to be 15, which are in good agreement

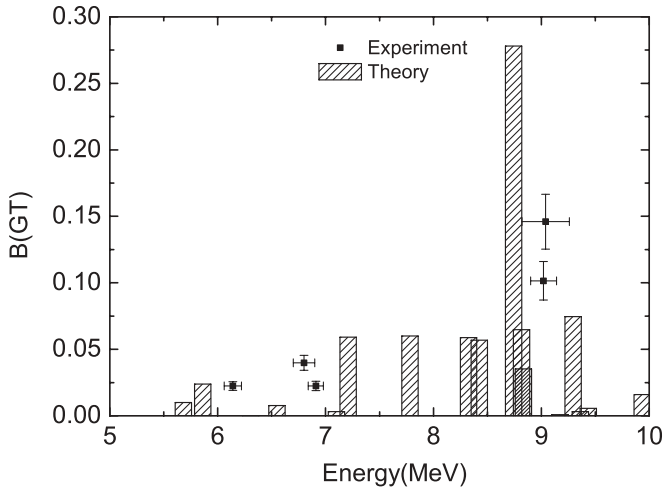

FIG. 12. The shell-model calculation of B(GT) values, as a function of excited energy of ^{21}O, for the allowed β decay of ^{21}N, in comparison to the experimental values.

with the present experimental values of $90.5 \pm 4.2\%$ and 13, respectively.

The experimentally deduced Gamow-Teller strengths for ^{21}N β decay to the observed states of ^{21}O are also compared to the shell-model calculations, as shown in Fig. 12. The calculated large B(GT) value at about 8.7 MeV is due to the large matrix element for the mother-sd to daughter-sd shell transition. Only a qualitative description is achieved, which implies that more theoretical, as well as experimental, efforts are needed to understand the details of the excited state structure of the neutron-rich unstable nuclei.

IV. SUMMARY

For the first time spectroscopic information is obtained for the β-decay chain of ^{21}N based on β-n, β-γ, and β-n-γ coincidence measurements. Thirteen new neutron groups, ranging from 0.28 to 4.98 MeV, are observed with a total neutron emission branching ratio of $90.5 \pm 4.2\%$. A half-life of 82.9 ± 7.5 ms is determined for the β decay of ^{21}N, in agreement with previous measurements. The level scheme of ^{21}O is established up to about 9 MeV excitation energy and the spin-parity values of five excited states following the neutron emission of ^{21}O are assigned. A preliminary shell-model calculation is performed and compared to the experimental data.

ACKNOWLEDGMENTS

We would like to acknowledge the staff of HIRFL for providing the ^{26}Mg primary beam and the staff of RIBLL for all kinds of assistance. This work is supported by the National Basic Research Program (973 program) of China (2007CB815002) and the National Natural Science Foundation of China (10775003, 10475004, 10735010, 10775005, 10875002, and 10827505).

[1] O. Sorlina and M.-G. Porquet, Prog. Part. Nucl. Phys. **61**, 602 (2008).
[2] K. W. Scheller, J. Görres, J. G. Ross, M. Wiescher, R. Harkewicz, D. J. Morrissey, B. M. Sherrill, M. Steiner, N. A. Orr, and J. A. Winger, Phys. Rev. C **49**, 46 (1994).
[3] C. S. Sumithrarachchi, D. W. Anthony, P. A. Lofy, and D. J. Morrissey, Phys. Rev. C **74**, 024322 (2006).
[4] Z. H. Li *et al.*, Phys. Rev. C **72**, 064327 (2005).
[5] J. L. Lou *et al.*, Phys. Rev. C **75**, 057302 (2007).
[6] A. C. Mueller *et al.*, Nucl. Phys. **A513**, 1 (1990).
[7] P. L. Reeder, Y. Kim, W. K. Hensley, H. S. Miley, R. A. Warner, Z. Y. Zhou, D. J. Vieira, J. M. Wouters, and H. L. Siefert, in *Proceedings of the International Conference on Exotic Nuclei and Atomic Masses, Arles, France, 19–23 June 1995*, edited by M. de Saint Simon and O. Sorlin (Editions Frontieres, Gif-sur-Yvette, France, 1995), p. 587.
[8] W. N. Catford *et al.*, Nucl. Phys. **A503**, 263 (1989).
[9] M. Stanoiu *et al.*, Phys. Rev. C **69**, 034312 (2004).
[10] Z. Sun, W. L. Zhan, Z. Y. Guo, G. Xiao, and J. X. Li, Nucl. Instrum. Methods Phys. Res. A **503**, 496 (2003).
[11] Q. Y. Hu, Y. L. Ye, Z. H. Li, X. Q. Li, D. X. Jiang, T. Zheng, Q. J. Wang, H. Hua, C. E. Wu, Z. Q. Chen, J. Ying, D. Y. Pang, G. L. Zhang, and J. Wang, IEEE Trans. Nucl. Sci. **52**, 473 (2005).
[12] J. L. Lou *et al.*, Nucl. Instrum. Methods Phys. Res. A **606**, 645 (2009).
[13] R. A. Cecil *et al.*, Nucl. Instrum. Methods Phys. Res. A **161**, 439 (1979).
[14] J. X. Dong *et al.*, Nucl. Elect. Detect. Tech. **19**, 4 (1999).
[15] http://www.nndc.bnl.gov/ensdf.
[16] J. W. Olness, E. K. Warburton, and D. E. Alburger, Nucl. Phys. **A378**, 539 (1982).
[17] B. A. Brown, A. Etchegoyen, and W. D. M. Rae, computer code OXBASH, MSU-NSCL Report No. 524, 1988.